AIAA JOURNAL
Vol. 31, No. 11, November 1993

Developing Numerical Techniques for Solving Low Mach Number Fluid-Acoustic Problems

Vincent P. Manno* and Scott H. Reitsma†
Tufts University, Medford, Massachusetts 02155
and
Thomas F. Tureaud‡
Charles Stark Draper Laboratories, Inc., Cambridge, Massachusetts 02139

Numerical techniques applicable to the solution of low Mach number ($M < 0.1$) fluid-acoustic problems are addressed. Conservation equations applicable to this regime are derived by applying four simplifying assumptions to the fully compressible form of the Navier-Stokes and energy equations: isentropic state changes, adiabatic flow, negligible density variation inertial terms, and Stokes' hypothesis. The resulting equations, termed acoustic compressible, are similar to the traditional pseudocompressible equations except for two distinctions. Pseudocompressible solutions use artificially high Mach numbers for computational convenience and neglect the pressure convection term in the mass conservation equation. Whether a pseudocompressibility method using physically correct Mach numbers can be used as a substitute for the more complex acoustic compressible equation set is addressed theoretically and through the numerical solution of unsteady incompressible and fluid-acoustic test problems. The results show that the pseudocompressibility method can be used to recover temporal accuracy in incompressible problems as long as the characteristic time scales are sufficiently faster than bulk flow time scales. The simulation of acoustic wave propagation through a shear layer shows that temporal accuracy in the fluid-acoustic regime requires exact Mach number specification. Using the pseudocompressible equations in this problem introduces spatially dependent propagation speeds and inaccurate eigensystems. These discrepancies are of greatest concern at higher Mach numbers ($M > 0.1$), and they appear to be due to the neglect of the pressure convection term in the pseudo-compressible formulation.

Nomenclature

In the body of the paper, symbols marked with a caret (e.g., $\hat{U}$) are dimensional. All other symbols (e.g., U) are dimensionless.

A_x = x-direction convection Jacobian
c = pressure wave propagation speed
c_{ac} = acoustic compressible c
c_{obs} = c observed in numerical tests
c_{pc} = pseudocompressible c
c_0 = speed of sound
e = specific internal and kinetic energy
F = p' amplitude function
G = v' amplitude function
h = specific enthalpy
i = $\sqrt{-1}$
k = wave number
k_T = thermal conductivity
L = characteristic length
M = Mach number, U/c
M_0 = reference Mach number, U_0/c_0
M_1 = Mach number at $y = 1$
M' = $\partial M/\partial y$
p = pressure
p_{back} = back pressure
p_e = imposed pressure fluctuation
p_{ref} = reference pressure
p_{up}^n = upstream p at time index n
p_0 = reference downstream pressure
p^+ = pressure term defined in Eq. (15)
p' = pressure perturbation
Re = Reynolds number, $\rho_0 U_0 L/\mu$
$(\ )_s$ = isentropic condition
T = temperature
t = time
$U(U)$ = velocity vector, magnitude
U_0 = reference velocity magnitude
u = x-direction component of U
u_{up}^n = upstream u at time index n
u' = perturbation of u
v = y-direction component of U
v' = perturbation of v
X = right eigenvector matrix of A_x
x = horizontal coordinate
y = vertical coordinate
β = pseudocompressibility factor
κ = shear layer problem eigenvalue
λ = wavelength
λ_x = eigenvalues of A_x
μ = absolute viscosity
μ' = second viscosity coefficient
ρ = density
ρ_0 = reference density
τ = shear stress tensor
ϕ = phase lag
ω = frequency
ω_c = critical frequency

I. Introduction

THIS paper addresses techniques for simulating fluid-acoustic phenomena in subsonic flow of low compressibility fluids. A fundamental aspect of fluid acoustics is the wide spectrum of relevant physical time scales and propagation speeds. In a problem with a predominant length scale of order $\hat{L}$, bulk flow fluid transients evolve with a time scale on the order of $\hat{L}/\hat{U}$. Acoustic waves have time scales on the order of $\hat{L}/\hat{c}$. The ratio of these time scales is the Mach number ($M = \hat{U}/\hat{c}$).

Received Aug. 11, 1992; revision received Feb. 23, 1993; accepted for publication Feb. 24, 1993.
*Associate Professor, Department of Mechanical Engineering.
†Ph.D. Candidate, Department of Mechanical Engineering.
‡Senior Member Technical Staff, M/S 20, 555 Technology Square.

M can be used to categorize flow regimes. In high M ($\gg 0$), aeroacoustic problems, bulk flow velocities and acoustic wave propagation speeds are of similar magnitude. This implies a conservation equation set with a relatively narrow range of eigenvalues or low "stiffness." This similarity of time scales allows efficient numerical tracking of both pressure propagation and bulk flow transient evolution. The simulation challenges in this regime are due to shock waves, viscous dissipation, and nonisentropic thermodynamic processes which are negligible in low speed flows.

Unsteady, low M ($\ll 1$) flows are characterized by a wider range of time scales. Whether all time scales are important is problem dependent. Consider the following three approaches to unsteady, low M problems. The first is incompressible flow in which the bulk motion temporal behavior is of interest and pressure wave propagation is of no concern. Pressure can be a function of time and space in these problems but pressure wave propagation speeds are limited to convective velocities (e.g., Tollmein-Schlichting waves). The second category is decoupled fluid-acoustic analysis. This approach is exemplified by Lighthill's acoustic analogy[1] in which acoustic source production is due solely to incompressible turbulent flow effects (Reynolds stresses) but propagation and dissipation of these waves through the fluid is modeled independently of the fluid dynamics. Hence, the fluid dynamics and the acoustic dynamics do not "interact." Current computational methods have been applied successfully to both of these approaches.[2-4]

The third category of problems involves coupled fluid motion and acoustic phenomena. Examples include acoustic control of boundary-layer transition,[5] the interaction of edgetones,[6] and the harmonic feedback observed in vortex shedding from transitional flow over an airfoil.[7] In the latter example, which has been observed experimentally but never simulated from first principles, an acoustic signal due to the shedding of Tollmein-Schlichting instability waves at the airfoil trailing edge is modified to yield distinct tonals due to the interaction of the acoustic waves with the instability receptivity zone upstream on the airfoil surface.

The next section addresses conservation equations and their implications. It includes the description of an equation set, termed "acoustic compressible," which might be viewed as a compromise between the incompressible and fully compressible flow assumptions. The acoustic compressible equations are similar to the traditional pseudocompressible equations except for M assumptions (pseudocompressibility factor) and the retention of the pressure convection term in the former. These differences are investigated theoretically and through numerical experiments using a pseudocompressible code.

II. Conservation Equation Sets: Physics and Numerics

A. Background

The fully compressible Navier-Stokes equations combined with energy conservation and an equation of state [Eqs. (1-5)] constitute the correct starting point for fluid-acoustic analysis. The equations are presented in two-dimensional, Cartesian coordinates for ease of explanation, and extension to other coordinate systems does not introduce new concepts.

$$\frac{\partial \hat{\rho}}{\partial \hat{t}} + \frac{\partial(\hat{\rho}\hat{u})}{\partial \hat{x}} + \frac{\partial(\hat{\rho}\hat{v})}{\partial \hat{y}} = 0 \tag{1}$$

$$\frac{\partial(\hat{\rho}\hat{u})}{\partial \hat{t}} + \frac{\partial(\hat{\rho}\hat{u}^2)}{\partial \hat{x}} + \frac{\partial(\hat{\rho}\hat{u}\hat{v})}{\partial \hat{y}} = -\frac{\partial \hat{p}}{\partial \hat{x}} + \hat{\mu}\left\{\frac{\partial^2 \hat{u}}{\partial \hat{x}^2} + \frac{\partial^2 \hat{u}}{\partial \hat{y}^2} + \frac{\partial}{\partial \hat{x}}[\mathrm{div}(\hat{U})]\right\} + \frac{\partial}{\partial \hat{x}}[\hat{\mu}'\mathrm{div}(\hat{U})] \tag{2}$$

$$\frac{\partial(\hat{\rho}\hat{v})}{\partial \hat{t}} + \frac{\partial(\hat{\rho}\hat{u}\hat{v})}{\partial \hat{x}} + \frac{\partial(\hat{\rho}\hat{v}^2)}{\partial \hat{y}} = -\frac{\partial \hat{p}}{\partial \hat{y}} + \hat{\mu}\left\{\frac{\partial^2 \hat{v}}{\partial \hat{x}^2} + \frac{\partial^2 \hat{v}}{\partial \hat{y}^2} + \frac{\partial}{\partial \hat{y}}[\mathrm{div}(\hat{U})]\right\} + \frac{\partial}{\partial \hat{y}}[\hat{\mu}'\mathrm{div}(\hat{U})] \tag{3}$$

$$\frac{\partial(\hat{\rho}\hat{e})}{\partial \hat{t}} + \frac{\partial(\hat{\rho}\hat{u}\hat{h})}{\partial \hat{x}} + \frac{\partial(\hat{\rho}\hat{v}\hat{h})}{\partial \hat{y}} = \hat{k}_T(\nabla^2 \hat{T}) + \nabla \cdot (\hat{\tau} \cdot \hat{U}) \tag{4}$$

$$\hat{\rho} = \mathrm{f}(\hat{p}, \hat{T}) \tag{5}$$

These equations imply that density variations are significant for both state changes and inertial effects, that energy conservation must include flow work and viscous dissipation, and that processes are tightly coupled through the equation of state. They are a hyperbolic-parabolic mathematical system, and the eigenvalues of the x-direction, inviscid flux Jacobian are $\hat{u}$, $\hat{u} + \hat{c}$, and $\hat{u} - \hat{c}$ with analogous values in the y direction. The propagation speed $\hat{c}$ appearing in the eigenvalues is not a function of local bulk velocity $\hat{u}$. The numerical solution of these equations becomes less tractable at low M (<0.1) since the various matrices associated with the discretized problems become ill conditioned.

Subsonic, low compressibility flows (e.g., water) allow certain simplifying assumptions. These may be understood by writing Eq. (1) in the form

$$\left(\frac{\partial \hat{\rho}}{\partial \hat{p}}\right)\frac{\partial \hat{p}}{\partial \hat{t}} + \hat{\rho}\left[\frac{\partial \hat{u}}{\partial \hat{x}} + \frac{\partial \hat{v}}{\partial \hat{y}}\right] + \hat{u}\left(\frac{\partial \hat{\rho}}{\partial \hat{p}}\right)\frac{\partial \hat{p}}{\partial \hat{x}} + \hat{v}\left(\frac{\partial \hat{\rho}}{\partial \hat{p}}\right)\frac{\partial \hat{p}}{\partial \hat{y}} = 0 \tag{6}$$

If an isentropic state relation

$$\left(\frac{\partial \hat{\rho}}{\partial \hat{p}}\right) \approx \left(\frac{\partial \hat{\rho}}{\partial \hat{p}}\right)_s = \frac{1}{\hat{c}_0^2} \tag{7}$$

is substituted into Eq. (6) the following expression results:

$$\frac{\partial \hat{p}}{\partial \hat{t}} + \hat{\rho}\hat{c}_0^2\left[\frac{\partial \hat{u}}{\partial \hat{x}} + \frac{\partial \hat{v}}{\partial \hat{y}}\right] + \left[\hat{u}\frac{\partial \hat{p}}{\partial \hat{x}} + \hat{v}\frac{\partial \hat{p}}{\partial \hat{y}}\right] = 0 \tag{8}$$

It contains three terms: the local time rate of change of pressure, the change of pressure due to the dilation of the flow, and a "pressure convection" term.

Equation (8) can be used to put existing solution methods into perspective. For example, if $\hat{c}_0$ is assumed to approach infinity, Eq. (8) becomes the incompressible constraint

$$\frac{\partial \hat{u}}{\partial \hat{x}} + \frac{\partial \hat{v}}{\partial \hat{y}} = 0 \tag{9}$$

Equation (9), taken together with a momentum equation which ignores density changes in the inertial terms (Boussinesq assumption), can be solved numerically using "pressure correction" techniques.[8,9] These methods require auxiliary equations to link pressure and velocity since Eq. (9) removes the direct connection between these primitive variables. The incompressible equations can capture unsteady fluid motion, but acoustic pressure dynamics are lost. Hence, they are not applicable to coupled fluid-acoustic analysis.

B. Pseudocompressible Equations

A second class of solution techniques is obtained if only the third term of Eq. (8) is ignored and the second term is modified by replacing the physical term $\hat{\rho}\hat{c}_0^2$ with a control parameter usually represented by the symbol $\hat{\beta}$

$$\frac{\partial \hat{p}}{\partial \hat{t}} + \hat{\beta}\left[\frac{\partial \hat{u}}{\partial \hat{x}} + \frac{\partial \hat{v}}{\partial \hat{y}}\right] = 0 \tag{10}$$

where $\hat{\beta}$ is the "pseudocompressibility" factor. In the pseudocompressibility equations, pressure and velocity are linked directly. The control parameter $\hat{\beta}$ is reduced from its physical value (equivalent to artificially increasing M) in order to reduce equation set stiffness. The basic concept was developed by Chorin[10] for the steady-state solution of the incompressible Navier-Stokes equations. The steady-state solution procedure is to solve the system using a false transient approach continuing in pseudotime until the pressure time derivative approaches zero, which in turn implies a divergence-free velocity field.

If the technique is applied to fluid-acoustic problems, by advancing the pseudocompressibility equations in real time, accuracy would be compromised because of distortion of the relative pressure wave to convective time scales. Consider that the pseudocompressible x-direction, inviscid flux Jacobian and its eigenvalues are

$$A_x = \begin{bmatrix} 0 & \hat{\beta} & 0 \\ 1/\hat{\rho} & 2\hat{u} & 0 \\ 0 & \hat{v} & \hat{u} \end{bmatrix} \tag{11a}$$

$$\hat{\lambda}_x = \hat{u}, \qquad \hat{u} \pm \sqrt{\hat{u}^2 + \hat{\beta}/\hat{\rho}} = \hat{u},\ \hat{u} \pm \hat{c}_{pc} \tag{11b}$$

These characteristics are different than those of the fully compressible equation set in that the effective propagation speed $\sqrt{\hat{u}^2 + \hat{\beta}/\hat{\rho}}$ depends on the x component of the local velocity u.

C. Acoustic Compressible Equations

Altering propagation speeds and neglecting the pressure convection term cannot be assumed to be appropriate for fluid-acoustic simulation. These deficiencies could be addressed by using Eq. (8) in its entirety coupled to a Boussinesq momentum conservation equation in which Stokes' hypothesis is invoked. (The bulk coefficient of viscosity, $\hat{\mu}'$, is unimportant for frequencies below several kilohertz.[11]) These assumptions define the acoustic compressible equations. If the equations are nondimensionalized using a characteristic length $\hat{L}$, a reference velocity $\hat{U}_0$, a characteristic time $(\hat{L}/\hat{U}_0)$, a reference density $\hat{\rho}_0$, and a reference pressure $\hat{\rho}_0\hat{c}_0^2$, the result is

$$\frac{\partial p^+}{\partial t} + \frac{\partial (p^+ u)}{\partial x} + \frac{\partial (p^+ v)}{\partial y} = 0 \tag{12}$$

$$\frac{\partial (p^+ u)}{\partial t} + \frac{\partial (p^+ u^2)}{\partial x} + \frac{\partial (p^+ uv)}{\partial y} = -\frac{1}{M_0^2}\frac{\partial p^+}{\partial x} + \frac{1}{Re}\left[\frac{\partial^2 u}{\partial x^2} + \frac{\partial^2 u}{\partial y^2}\right] \tag{13}$$

$$\frac{\partial (p^+ v)}{\partial t} + \frac{\partial (p^+ uv)}{\partial x} + \frac{\partial (p^+ v^2)}{\partial y} = -\frac{1}{M_0^2}\frac{\partial p^+}{\partial y} + \frac{1}{Re}\left[\frac{\partial^2 v}{\partial x^2} + \frac{\partial^2 v}{\partial y^2}\right] \tag{14}$$

$$p^+ = \frac{[\hat{p} - \hat{p}_{ref} + \hat{\rho}_0\hat{c}_0^2]}{\hat{\rho}_0\hat{c}_0^2} \tag{15}$$

A flux form is used in fluid-acoustic problems because it allows the utilization of hyperbolic numerical solution methods such as flux differencing.[12] This approach, although attractive from most perspectives, introduces problems in treating viscous terms and in formulating boundary conditions. Using Eqs. (12–15), the x-direction, inviscid flux Jacobian of the acoustic compressible equation set is

$$A_x = \begin{bmatrix} 0 & 1 & 0 \\ \dfrac{1}{M_0^2} - u^2 & 2u & 0 \\ -uv & v & u \end{bmatrix} \tag{16}$$

where $M_0 = \hat{U}_0/\hat{c}_0$. The eigenvalues are u, $u \pm (1/M_0)$.

Whereas solving the acoustic compressible equations would be computationally intensive for nonfluid-acoustic problems, it does represent a reasonable model of pressure wave propagation. Also, its simplifying assumptions may offer computational savings over a fully compressible formulation in low M, fluid-acoustic problems.

D. Acoustic Compressible vs Pseudocompressible Formulations

Comparison of the acoustic compressible and pseudocompressible equation sets shows that they are similar except for inconsistent values of M and the omission of the pressure convection term $(U \cdot \nabla p)$. These differences are reflected in the eigensystems and the transport which they embody. Similar to the fully compressible equations, the acoustic compressible eigenvalues contain pressure wave propagation speeds which are independent of the local velocity. In contrast, the eigenvalues of the pseudocompressible equation set [see Eq. (11b)] contain propagation speeds which depend on the local velocity. The eigenvectors of the two equation sets are also different.[13]

The utility of the acoustic compressible approach can only be assessed in practice. As a first step in this assessment, its distinctions from pseudocompressibility can be gauged by using a pseudocompressibility code with β as a control parameter. Relevant sensitivities include exacerbation of spatial truncation errors due to high (i.e., physical) values of β, increased equation set stiffness, distortion of waves due to local velocity dependent wave speeds, and pressure wave amplitude and phase errors due to the neglect of the pressure convection term.

The DTNS code[14] was chosen as the baseline pseudocompressible code for these simulations. It is a finite-volume, primitive variable code which produces steady-state solutions of the incompressible Navier-Stokes equations using a (pseudo-) time marching, hyperbolic algorithm. Thus, its basic structure can be used for unsteady solutions if physically reasonable values of β are employed. The code uses upwind differencing schemes based upon the flux difference split discretizations described by Chakravarthy and Osher.[15] Flux limiters were not invoked since they appear to distort the wave propagation.

The original DTNS code utilized either explicit Runge-Kutta or implicit, approximately factored time advancement algorithms. It has been reported that approximate factorization solutions combined with high values of β produce large temporal truncation errors.[16] Therefore, either explicit or nonfactored, implicit techniques are required. Nonfactored, implicit techniques have high computational overheads per time step which makes them worthwhile only if large time steps can be used. However, in fluid-acoustic simulations, the time steps are limited to Courant-Friedrichs-Lewy (CFL) numbers (based on the speed of sound) on the order of unity due to the need to properly capture acoustic wave propagation. Hence, only explicit methods are used. It should be noted that explicit algorithms are more easily adapted to vector computer calculations. Finally, the code was modified in this work to allow time-dependent boundary conditions.

III. Results and Discussion

This paper reports the results of the first three of an ongoing series of test problems. The first problem is steady driven cavity flow at low Re. Although it is neither unsteady nor acoustic (at low Re), it is used to assess the impact of higher values of β on the asymptotic truncation errors in the converged solution. The second problem is an oscillating inviscid, nonacoustic flow in a duct. It has an analytic solution if incompressible flow is assumed. It is used to determine what values of β are required for the pseudocompressibility method to recover time-accurate results in the incompressible domain. The third problem is the propagation of an acoustic wave through a shear layer. This has an analytic solution which is based on retaining the pressure convection term in the continuity equation. Hence, the pseudocompressible results can be compared to the analytic solution and discrepancies between the two can be assessed from the perspective of including (acoustic compressible equations) or excluding (pseudocompressible equations) the pressure convection term.

A. Driven Cavity Problem

Benchmark results for a square, lid-driven cavity at $Re = 100$, which agreed with the published solutions,[17] were obtained using $\beta = 1$ and a uniform 153×153 grid. A sensitivity study of the effect of β was then undertaken using various coarser grids. The value of β affects this steady-state problem

by amplifying the truncation errors associated with the numerical solution procedure. When using upwind, flux-difference numerical procedures, β appears in the left and right eigenvectors of the Jacobian matrix; hence, β influences not only the continuity equation but the momentum equations as well. Rogers[13] found that truncation errors in the momentum equations grew as the square root of β. Although similar trends were noted in the set of calculations described herein, it was also found that the errors introduced were negligible even at high β (= 10,000) when a reasonably fine grid was used.[18] This is important since fluid-acoustic problems usually require finer grids than most other unsteady simulations.

B. One-Dimensional Channel with Variable Back Pressure

The second test problem is unsteady flow of an inviscid, incompressible fluid through a one-dimensional channel subject to an oscillatory back pressure. This problem, which is illustrated in Fig. 1, has been used by others to assess transient solution methods.[2,13] A constant total pressure ($p_t = p + \rho u^2/2$) boundary condition is imposed at the upstream side ($x = 0$), and the following time varying static pressure is set at the downstream end ($x = 1$)

$$p_{\text{back}} = p_0 + p_e \sin(\omega t) \tag{17}$$

In this study, $p_t = 1.5$, $p_0 = 1.0$, and $p_e = 0.1$. The flow and pressure fields associated with $\omega = 0$ are taken as the initial conditions.

In the limit of small pressure oscillations ($p_e \ll p_0$), the analytic solution[2] takes the following form:

$$u(t) = 1 - \frac{p_e}{1+\omega^2}\left[\sin(\omega t) - \omega\cos(\omega t) + \omega\exp(-t)\right] \tag{18a}$$

$$p(x,t) = p_0 + p_e\sin(\omega t) + \frac{(x-1)p_e\omega}{1+\omega^2}\left[\cos(\omega t) + \omega\sin(\omega t) - \exp(-t)\right] \tag{18b}$$

Equations (18a) and (18b) contain a decaying exponential startup transient and asymptotic harmonic motion. Pressure is a function of both x and t whereas velocity is a function of t only. Velocity is not a function of x due to the incompressible assumption. From the analytic solutions, an expression for the phase shift between pressure and velocity can be developed as a function of ω,

$$\phi = 180 \text{ deg} - \tan^{-1}(\omega) \tag{19}$$

At low values of ω, pressure and velocity are completely out of phase (defined as a velocity lead of 180 deg). At high values of ω, velocity leads pressure by 90 deg.

The computational grid consisted of square cells: 40 in the streamwise x direction and two in the cross stream y direction.

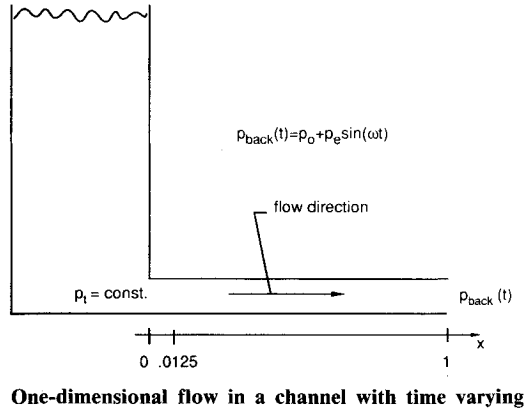

Fig. 1 One-dimensional flow in a channel with time varying back pressure, problem schematic.

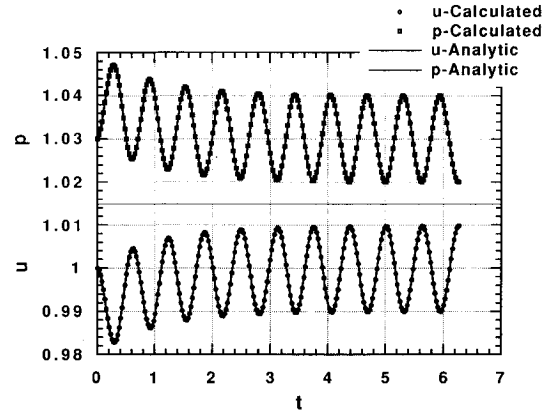

Fig. 2 Comparisons of calculated vs analytic solutions for $\omega = 10$ using $\beta = 10{,}000$ at $x = 0.0125$.

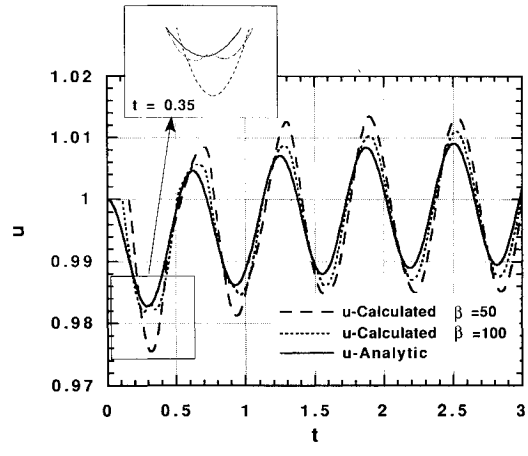

Fig. 3 Comparison of calculated vs analytic solutions for $\omega = 10$ using lower values of β at $x = 0.0125$.

All vertical gradients were set to zero at the upper and lower boundaries. The constant total pressure upstream boundary condition was implemented by specifying the static pressure at the boundary based on the calculated velocity at the previous time step

$$p_{\text{up}}^{n+1} = p_t - \tfrac{1}{2}\rho(u_{\text{up}}^n)^2 \tag{20}$$

An explicit time advancement scheme was used. The computational time step was varied inversely with $\sqrt{\beta}$ and the one-dimensional CFL number ($\Delta t\sqrt{\beta} + u^2/\Delta x$) was set to approximately 0.50.

Computations were performed over a range of ω and β. It was expected that high values of β would be required to approximate the infinite wave speeds of the incompressible analytic solution. Also, higher values of β should be needed to capture high-frequency phenomena whereas lower values of β should suffice to simulate low-frequency cases. Primitive variables at $x = 0.0125$ (see Fig. 1) were monitored. Figure 2 compares calculated and analytic results for $\omega = 10$ using $\beta = 10{,}000$. The agreement is excellent in both the initial transient and the asymptotic harmonic motion. Figure 3 shows the same case ($\omega = 10$) computed at lower values of β. Significant departure from the analytic solution is apparent. The coupling between pressure and velocity has been affected such that $\partial u/\partial x$ is artificially high for a given $\partial p/\partial t$ [see Eq. (10)]. This causes the velocity to overshoot the analytic value.

At the lower wave speeds (low values of β), wave interactions are observable. For example in Fig. 3 at $t = 0.35$ for $\beta = 100$, the unusual waveform is caused by the initial wavefront traveling the length of the channel, reflecting off the constant total pressure boundary, and interacting with an

oncoming wave. In the incompressible analytic solution, these interactions happen instantaneously. In the high β calculation (see Fig. 2) these interactions are nearly instantaneous and are not noticeable.

There is a finite signal transit speed associated with the pseudocompressible solution. As shown in Fig. 3, the velocity at $x = 0.0125$ remains undisturbed until the first pressure wave reaches that point (i.e., $t = 0.2$ for $\beta = 50$). Also, the velocity response shows a noticeable delay compared to the analytic solution (the low β curves are offset to the right) which persists throughout the transient. In contrast, the conditions at $x = 0.0125$ in the incompressible analytic solution are affected instantaneously by the back pressure. The initial delay in the computed signal response can be predicted by the characteristics of the pseudocompressible equations. That is,

$$\text{time delay} = \frac{\text{distance}}{(\text{wave propagation speed} - u)} = \frac{(1-0.0125)}{\sqrt{\beta+1}-1} \quad (21)$$

Figure 4 shows a comparison between the predicted [Eq. (21)] and observed time delays. Table 1 compares the observed propagation speeds to the propagation speeds of the pseudocompressibility method [see Eq. (11)]. A column showing the physically correct propagation speeds, as would be calculated by the acoustic compressibility method, is also included. The uncertainty in c_{obs} is due to numerical dispersion which distorts the shape of the wave front and makes the determination of wave timing difficult. In nearly all cases, the observed propagation speeds agree, within uncertainty, with the expected pseudocompressible speeds. Pseudocompressibility predicts nearly correct wave propagation speeds for problems when the M is below 0.1 (i.e., $\beta > 100$).

Figure 5 presents the phase shift between the velocity (at $x = 0.0125$) and the back pressure. In the analytic incompress-

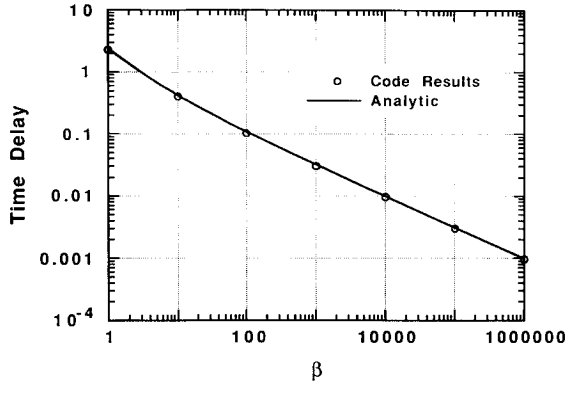

Fig. 4 Comparison of predicted [Eq. (21)] vs observed signal transit time delays.

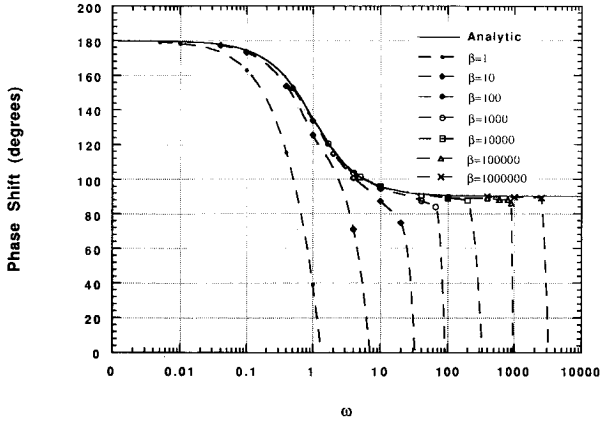

Fig. 5 Pressure/velocity phase shift as a function of ω and β.

Table 1 Comparison of expected and observed propagation speeds

β	c_{obs}	c_{pc}	c_{ac}
1	1.433 ±0.02	1.414	1.000
10	3.420 ±0.11	3.317	3.162
100	10.50 ±0.60	10.05	10.00
1,000	33.27 ±1.98	31.64	31.62
10,000	102.2 ±3.00	100.0	100.0
100,000	326.9 ±6.30	316.2	316.2
1,000,000	1,025.0 ±21.0	1,000.0	1,000.0

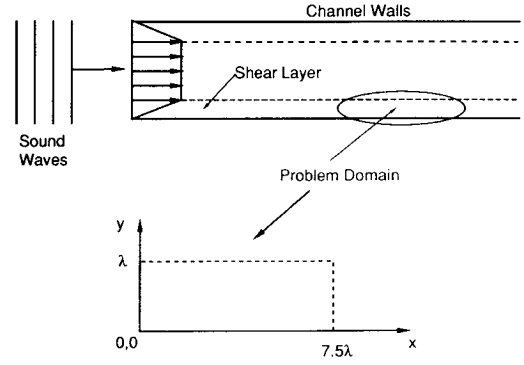

Fig. 6 Propagation of a planar acoustic wave through a linear gradient shear layer.

ible solution boundary condition time scales cannot be shorter than the (infinite) pressure propagation speeds. When ω is small, the time scale of the pressure boundary condition is long and low values of β yield accurate, "incompressible" solutions. When ω is increased, the time scale of the pressure boundary condition becomes shorter, requiring higher values of β. In other words, a value of β must be used that is high enough to keep the wave propagation time scales sufficiently shorter than other relevant problem time scales.

C. Acoustic Propagation Through a Shear Layer

The third test problem is the propagation of an acoustic signal through a shear layer. This is a true fluid-acoustic problem. An analytic perturbation solution to this problem based upon the simplifying assumptions of a unidirectional, unperturbed flow in the x direction was presented by Pridmore-Brown,[19] and to date this problem has only been solved numerically using fully compressible assumptions.[20] The analytic solution includes the pressure convection term.

A problem schematic is shown in Fig. 6. The domain spans only the shear layer, which is assumed to be of constant thickness (height) over the horizontal extent. The baseline flow condition is a horizontal velocity profile $U(y)$, which rises linearly from 0 at $y = 0$ to the freestream M_1 at $y = 1$. Using an isentropic flow assumption, the time-dependent perturbations of horizontal velocity component (u'), vertical velocity component (v'), and pressure (p') obey the following equations:

$$\frac{1}{c_0^2}\left(\frac{\partial p'}{\partial t}\right) + \frac{U}{c_0^2}\left(\frac{\partial p'}{\partial x}\right) + \rho_0\left[\frac{\partial u'}{\partial x} + \frac{\partial v'}{\partial y}\right] = 0 \quad (22)$$

$$\frac{\partial u'}{\partial t} + U\frac{\partial u'}{\partial x} + v'\frac{\partial U}{\partial y} + \frac{1}{\rho_0}\left(\frac{\partial p'}{\partial x}\right) = 0 \quad (23)$$

$$\frac{\partial v'}{\partial t} + U\frac{\partial v'}{\partial x} + \frac{1}{\rho_0}\left(\frac{\partial p'}{\partial y}\right) = 0 \quad (24)$$

This equation set is actually a perturbation form of the acoustic compressible equations. The pressure convection

term is the second term of Eq. (22). When Eqs. (22–24) are combined, a "wave equation" of the form

$$\frac{1}{c_0^2}\left(\frac{\partial^2 p'}{\partial t^2}\right) = (1-M^2)\frac{\partial^2 p'}{\partial x^2} + \frac{\partial^2 p'}{\mathrm{d}y^2} - \frac{2M}{c_0}\left(\frac{\partial^2 p'}{\partial x \partial t}\right) + 2\rho_0 c_0 \frac{\partial M}{\mathrm{d}y}\left(\frac{\partial v'}{\mathrm{d}x}\right) \tag{25}$$

results. In the case of small perturbations, a solution of the form

$$p' = F(\kappa, y)\, e^{ik(\kappa x - c_0 t)} \tag{26a}$$

$$v' = G(\kappa, y)\, e^{ik(\kappa x - c_0 t)} \tag{26b}$$

is applicable where F and G are amplitude functions. These solutions have a linear dispersive form[21] with a position independent phase speed equal to c_0/κ. When Eq. (26) is substituted into Eq. (25) and Eq. (24) is used to eliminate G, a second-order differential equation for the pressure amplitude function $F(\kappa, y)$ results

$$\frac{\mathrm{d}^2 F}{\mathrm{d}y^2} + \frac{2\kappa M'}{1-\kappa M}\left(\frac{\mathrm{d}F}{\mathrm{d}y}\right) + k^2[(1-\kappa M)^2 - \kappa^2]F = 0 \tag{27}$$

where $M' = \partial M/\partial y$. Equation (27) defines an eigenvalue problem in κ subject to the boundary conditions that $\mathrm{d}F/\mathrm{d}y = 0$ at $y = 0$ and $y = 1$. The eigenvalues are a function of wave number (k) and M_1. The solution of Eqs. (26) and (27) provide the analytic benchmark to which the pseudocompressible calculations are compared.

The computations were performed at a fixed wave number ($k = 2\pi$) and a range of M_1. The largest value of κ, which corresponds to the lowest propagation mode, was used. The

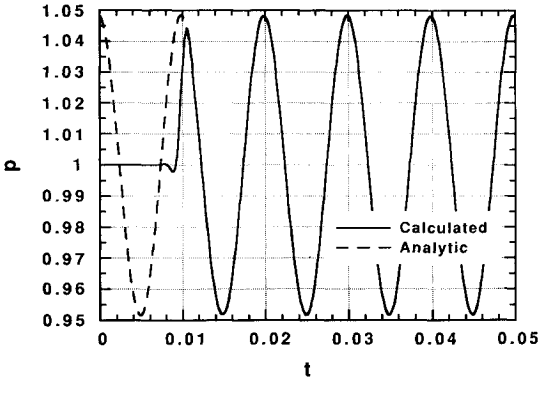

Fig. 7 Comparison of analytic and calculated pressure transients at $x = \lambda$, $y = \lambda/2$ for $M_1 = 0.01$.

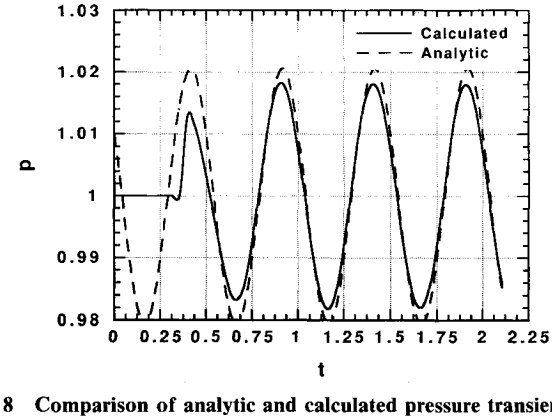

Fig. 8 Comparison of analytic and calculated pressure transients at $x = \lambda$, $y = \lambda/2$ for $M_1 = 0.50$.

Table 2 Input parameters for linear gradient, acoustic propagation problem

M_1	k	β	κ	$F(y=1)$
0.01	6.28319	10000	0.99508	0.04685
0.05	6.28319	400	0.97680	0.03657
0.10	6.28319	100	0.95660	0.02760
0.20	6.28319	25	0.92236	0.01707
0.30	6.28319	11.11	0.89327	0.01153
0.40	6.28319	6.25	0.86724	0.00830
0.50	6.28319	4	0.84316	0.00624

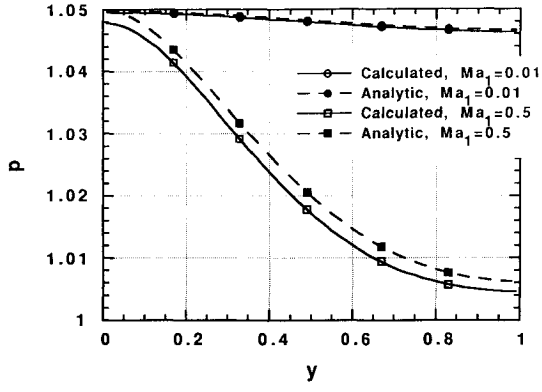

Fig. 9 Comparison of analytic and calculated pressure profiles across the shear layer at $t = 0.05$ for $Ma_1 = 0.01$, and $t = 1.92$ for $M_1 = 0.50$.

domain had unit height (i.e., $y_{max} = \lambda = 1$) and extended approximately 7.5 units horizontally. The horizontal length was chosen to allow the transient to progress for approximately 5 wave periods without the wave front reaching the downstream boundary. Cell dimensions of $\lambda/50$ produced grid independent solutions. The analytic solution was applied as the upstream boundary condition at $x = 0$, a zero pressure gradient was applied along the upper horizontal boundary, a slip condition (equal u and p, and opposite sign but equal magnitude v across the boundary cell interfaces) was applied along the lower horizontal boundary, and the unperturbed linear velocity profile was applied at the downstream boundary. A slip condition at the lower boundary may appear contradictory to the shear layer specification, but using the same approach as Pridmore-Brown the shear layer is imposed as an upstream condition and is preserved by the boundary conditions. The linear velocity profile was used as the initial condition in the field. The maximum pressure perturbations were limited to 5%, which fell within the linear range of the analytic solution. This maximum value always occurs at the wall ($y = 0$). The value of β was set to $1/M_1^2$ and the solution was advanced in time using a second-order Runge-Kutta scheme with a CFL number of 0.25. The appropriate eigenvalue κ, the value of β, and the magnitude of the pressure perturbation specified at the edge of the shear layer ($y = 1$) to achieve the 5% maximum perturbations are listed in Table 2.

Figures 7 and 8 are time histories of the pressure at $x = \lambda$, $y = \lambda/2$ ($x = 1$, $y = 0.5$) for M_1 of 0.01 and 0.5, respectively. The analytic solutions are also shown in each plot. The response delay in the calculated solution is due to the signal transit time to that point. The low M_1 results exhibit excellent agreement with the analytic solution in terms of both phase and amplitude. The higher M_1 solutions show disagreement in that the calculated pressure signal contains both amplitude attenuation and phase lag errors. Figure 9 compares the analytic and calculated pressure profiles at specific times as a function of y at the same downstream position for $M_1 = 0.01$ and 0.50. In agreement with the analytic solutions, Fig. 9

Table 3 Comparison of expected and observed amplitude errors

	$y = 0.01$			$y = 0.50$			$y = 0.99$		
M_1	Eq. (29), %	Code, %		Eq. (29), %	Code, %		Eq. (29), %	Code, %	
0.01	−0.01	−0.53	±0.37	−0.50	−0.57	±0.01	−0.70	−0.98	±0.39
0.05	−0.50	−1.19	±1.53	−2.38	−1.48	±0.32	−4.60	−2.07	±2.07
0.10	−0.10	−1.16	±0.92	−4.55	−2.50	±0.09	−8.57	−5.09	±1.64
0.30	−0.27	−2.34	±1.52	−11.60	−7.00	±0.30	−19.49	−17.17	±6.47
0.50	−0.42	−3.53	±2.59	−16.64	−11.90	±0.63	−24.32	−28.79	±13.7

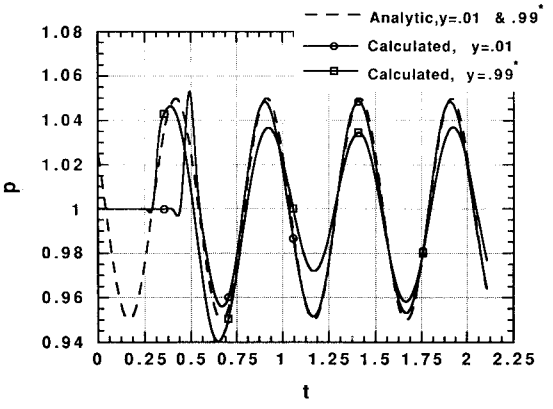

Fig. 10 Time response of pressure signal at $x = \lambda$ for two elevations $y = 0.01$ and $y = 0.99$; for $M_1 = 0.50$ (note that $y = 0.99$ curves marked by * have been scaled to match amplitudes at $y = 0.01$).

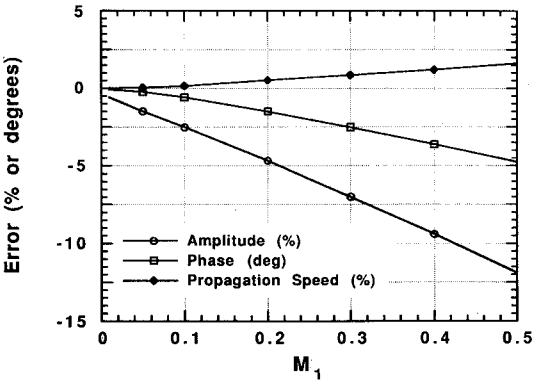

Fig. 11 Amplitude, phase, and phase speed errors of the pressure signal as a function of M_1 for $k = 2\pi$.

illustrates that sound pressure levels are concentrated near the wall at high M_1. The amplitude errors suggested in Fig. 8 are evident in Fig. 9.

Figure 10 contains the analytic and calculated time histories of pressure at $x = \lambda$ at two vertical elevations: near the wall ($y = 0.01$) and near the edge of the shear layer ($y = 0.99$). [Note that the $y = 0.99$ profiles have been magnified for clarity of comparison since amplitude variations at high M_1 are severe. This was done by multiplying the perturbations associated with both $y = 0.99$ curves by the ratio of $F(y = 1)$ for $Ma_1 = 0.01$ to $F(y = 1)$ for $M_1 = 0.50$ (see Table 2; magnification = 0.04685/0.00624 = 7.5).] As mentioned earlier, the analytic solution has a uniform phase speed c_0/κ across the shear layer. However, initially the calculated solution exhibits a different behavior. Figure 10 shows that the signal reaches the upper elevation before the lower elevation. This response is in approximate agreement with the eigenvalues of the pseudocompressible equation set. However, as the transient proceeds, the solution dynamics at the two elevations shift and take on a nearly identical constant phase speed very close to that imposed by the analytic boundary condition. In other words, the pseudocompressible equation set responds initially with its underlying hyperbolic characteristics, but as the upstream boundary condition drives the solution, the computed solution takes on the linear dispersive dynamics of the boundary condition. This readjustment is not due to any reflection since the first wave has not yet reached the downstream boundary at the time it occurs.

Another numerical experiment was run in which the time-dependent upstream boundary condition was changed to a steady-state boundary condition after one cycle. The upper elevation responded to this change in boundary condition faster than the lower elevation. The difference in the time responses could again be related to the local velocity dependent propagation speed of the pseudocompressible equations. This shows that once the time-dependent boundary condition was replaced with a steady-state boundary condition, the pseudocompressible solution reverted to its hyperbolic nature. Results analysis shows that β controls the initial response time but once the pressure signal arrives, the subsequent transient takes on the constant phase speed of the boundary condition. Understanding the relationship between information transmission and solution behavior in this class of problem is an important area for future investigation.

The departure of the computed results from the analytic solution can be used to assess the importance of the pressure convection term. As reported in Figs. 8–10, the pseudocompressible solution departs from the analytic solution as a function of M_1. A rederivation of Eq. (25) from Eqs. (22–24), but neglecting the pressure convection terms in Eq. (22), leads to the following modified equation:

$$\frac{1}{c_0^2}\left(\frac{\partial^2 p'}{dt^2}\right) = \frac{\partial^2 p'}{\partial x^2} + \frac{\partial^2 p'}{dy^2} - \frac{M}{c_0}\left(\frac{\partial^2 p'}{\partial x \partial t}\right) + 2\rho_0 c_0 \frac{\partial M}{dy}\left(\frac{\partial v'}{dx}\right) \quad (28)$$

which differs from Eq. (25) by the omission of the following two terms:

$$-M^2\left(\frac{\partial^2 p'}{\partial x^2}\right), \qquad -\frac{M}{c_0}\left(\frac{\partial^2 p'}{\partial x \partial t}\right)$$

Using the analytic solutions [Eq. (26)], the magnitude of the neglected terms can be compared to the left-hand side of Eq. (25). The resulting expression is

$$\text{amplitude error} \approx \frac{-M^2\left(\frac{\partial^2 p'}{\partial x^2}\right) - \frac{M}{c_0}\left(\frac{\partial^2 p'}{\partial x \partial t}\right)}{\frac{1}{c_0^2}\left(\frac{\partial^2 p'}{\partial t^2}\right)} = \kappa M(1 - \kappa M) \quad (29)$$

Since the right-hand side of Eq. (29) is always positive, the amplitude error should be an attenuation and the magnitude of the difference between the pseudocompressible and acoustic compressible solutions should increase with κM (for values of $\kappa M < 0.5$).

Figure 11 is a composite plot of the observed amplitude, phase, and propagation speed errors as a function of M_1 using the $x = \lambda$, $y = \lambda/2$ location as the monitoring point. The

figure indicates that all errors increase with increasing M_1. In congruence with Eq. (29), the amplitude errors are attenuations. The phase lags noted in the previous time history plots are also evident. Table 3 is a comparison of the expected [Eq. (29)] and calculated solution amplitude errors at a variety of M_1 at three elevations: $y = 0.01$, 0.50, and 0.99.

As predicted by Eq. (29), the errors increase in magnitude as both M_1 and elevation increase. Additional numerical experiments were run at $M_1 = 0.1$ for various wave numbers ($k = \pi$–6π). No systematic trends were observed. This is in agreement with Eq. (29) which shows that amplitude error is not a direct function of wave number. The calculated results do exhibit larger amplitude errors in the low bulk velocity region near the wall than that anticipated from Eq. (29).

An inference from these results is that the pressure convection term is unimportant for low M, fluid-acoustic problems. However, this must be tempered with the limitations of the specific test problem. First, this problem addresses only propagation of an acoustic signal and the strength and behavior of that signal are imposed from outside the simulation. Second, only a single propagation mode was imposed. This is different than a coupled fluid-acoustic problem in which the sound production and propagation are a direct result of flowfield-acoustic interactions.

IV. Concluding Remarks

This paper describes fluid-acoustic simulation techniques including a conservation equation set, termed acoustic compressible, to be used for such simulations. This equation set is similar to the traditional pseudocompressible approach. Since the pseudocompressible equations require less computational effort to solve, the question of whether they could be used as a surrogate for the acoustic compressible equations was explored. Similarities and differences between the pseudocompressible and acoustic compressible equation sets were identified theoretically and investigated numerically. Results demonstrate the importance of utilizing physically reasonable compressibility assumptions. The steady-state, driven cavity problem provided insight into the dependence of discretization errors on β. The transient, inviscid channel flow problem showed that in order to approximate an incompressible assumption, a value of β must be used which is high enough to keep the wave propagation time scale sufficiently small compared to the other problem time scales. If lower values of β are used, wave interactions that are not present in incompressible analyses can be obtained. The simulation of an acoustic wave propagating through a shear layer required specific values of β in order to match the analytic solution. The calculations provide evidence that the pressure convection term can be neglected and the pseudocompressible equations with physically correct values of β can be used in low M, fluid-acoustic problems.

Acknowledgments

The authors gratefully acknowledge the support of the Charles S. Draper Laboratory, Inc., under their IR&D and University Research programs. Some computations were performed on the NSF/Pittsburgh Supercomputing Center's Cray YMP computer under Grant CBT910018P. Also, the assistance of J. Gorski and H. Haussling of David Taylor Research Center in the acquisition and utilization of the DTNS code is appreciated.

References

[1]Lighthill, J., "On Sound Generated Aerodynamically I, General Theory," *Proceedings of the Royal Society,* Series A, Vol. 211A, March 1952, pp. 564–587.

[2]Merkle, C. L., and Athavale, M., "Time-Accurate Unsteady Incompressible Flow Algorithms Based on Artificial Compressibility," AIAA Paper 87-1137, June 1987.

[3]Rogers, S. E., and Kwak, D., "An Upwind Differencing Scheme for Time Accurate Incompressible Navier-Stokes Equations," *AIAA Journal,* Vol. 28, No. 2, 1990, pp. 253–262.

[4]Hardin, J. C., and Pope, D. S., "Sound Generation by a Stenosis in a Pipe," *AIAA Journal,* Vol. 30, No. 2, 1992, pp. 312–317.

[5]Saric, W. S., Hoos, J. A., and Radeztsky, R. H., "Boundary Layer Receptivity of Sound with Roughness," *Boundary Layer Stability and Transition to Turbulence,* edited by D. C. Reda, H. L. Reed, and R. Kobayashi, ASME FED-Vol. 114, American Society of Mechanical Engineers, New York, 1991, pp. 17–22.

[6]Crighton, D. G., "The Jet Edge-tone Feedback Cycle; Linear Theory For Operating Stages," *Journal of Fluid Mechanics,* Vol. 234, Jan. 1992, pp. 361–392.

[7]Goldstein, M. E., "Scattering of Acoustic Waves into Tollmein-Schlichting Waves by Small Streamwise Variations in Surface Geometries," *Journal of Fluid Mechanics,* Vol. 154, May 1985, pp. 509–529.

[8]Harlow, F. H., and Welch, J. E., "Numerical Calculation of Time-Dependent Viscous Incompressible Flow of Fluid with Free Surface," *Physics of Fluids,* Vol. 8, No. 12, 1965, pp. 2181–2189.

[9]Bentson, J., and Vradis, G., "Two-Stage Pressure Correction Technique for the Incompressible Navier-Stokes Equations," *AIAA Journal,* Vol. 28, No. 7, 1990, pp. 1155, 1156.

[10]Chorin, A. J., "A Numerical Method for Solving Incompressible Viscous Flow Problems," *Journal of Computational Physics,* Vol. 2, No. 1, 1967, pp. 12–26.

[11]Karin, S. M., and Rosenhead, L., "The Second Coefficient of Viscosity of Liquids and Gases," *Review of Modern Physics,* Vol. 24, No. 2, 1952, pp. 108–116.

[12]Roe, P. L., "Approximate Reimann Solvers, Parameter Vectors and Difference Schemes," *Journal of Computational Physics,* Vol. 43, No. 2, 1981, pp. 357–372.

[13]Rogers, S. E., "Numerical Solution of the Incompressible Navier-Stokes Equations," Ph.D. Thesis, Dept. of Aeronautics and Astronautics, Stanford Univ., Stanford, CA, March 1989.

[14]Gorski, J. J., "TVD Solutions of the Incompressible Navier-Stokes Equations with an Implicit Multigrid Technique," *Proceedings of the 1st National AIAA/ASME/SIAM/APS Fluid Dynamics Congress* (Cincinnati, OH), Vol. 1, AIAA, Washington, DC, 1988, pp. 394–401.

[15]Chakravarthy, S. R., and Osher, S., "A New Class of High-Accuracy TVD Schemes for Hyperbolic Conservation Laws," AIAA Paper 85-0363, Jan. 1985.

[16]Steger, J. L., and Kutler, P., "Implicit Finite-Difference Procedures for the Computation of Vortex Wakes," *AIAA Journal,* Vol. 15, No. 4, 1977, pp. 581–590.

[17]Ghia, U., Ghia, K. N., and Shin, C. T., "High-*Re* Solutions for Incompressible Flow Using the Navier-Stokes Equations and a Multigrid Method," *Journal of Computational Physics,* Vol. 48, No. 3, 1982, pp. 387–411.

[18]Reitsma, S. H., and Manno, V. P., "DTNS Test Matrix Results—Quadrants 1 and 2—Interim Report," Charles S. Draper Labs., Inc., CSDL-C-6231, Cambridge, MA, May 1991.

[19]Pridmore-Brown, D. C., "Sound Propagation in a Fluid Flowing Through an Attenuating Duct," *Journal of Fluid Mechanics,* Pt. 4, Aug. 1958, pp. 393–406.

[20]Hsieh, K.-C., "Assessment of Numerical Techniques for Unsteady Flow Calculations," AIAA Paper 89-1956-CP, June 1989.

[21]Whitham, G. B., *Linear and Nonlinear Waves,* Wiley, New York, 1974, pp. 9–12.